THE ASTROPHYSICAL JOURNAL, 554:281–290, 2001 June 10

OPTICAL COLOR GRADIENTS IN STAR-FORMING RING GALAXIES

VLADIMIR KORCHAGIN[1]
Institute of Physics, Stachki 194, Rostov-on-Don, Russia; vik@rsuss1.rnd.runnet.ru
Y. D. MAYYA
Instituto Nacional de Astrofisica, Optica y Electronica, Apdo Postal 51 y 216, C.P. 72000, Puebla, Mexico; ydm@inaoep.mx
AND
EDUARD VOROBYOV
Institute of Physics, Stachki 194, Rostov-on-Don, Russia; edik@rsuss1.rnd.runnet.ru
Received 1999 June 21; accepted 2001 February 15

ABSTRACT

We compute radial color gradients produced by an outwardly propagating circular wave of star formation and compare our results with color gradients observed in the classical ring galaxy, the "Cartwheel." We invoke two independent models of star formation in the ring galaxies. The first one is the conventional density wave scenario, in which an intruder galaxy creates a radially propagating density wave accompanied by an enhanced star formation following the Schmidt's law. The second scenario is a pure self-propagating star formation model, in which the intruder sets off only the first burst of stars at the point of impact. Both models give essentially the same results. Systematic reddening of $B-V$, $V-K$ colors toward the center, such as that observed in the Cartwheel, can be obtained only if the abundance of heavy elements in the star-forming gas is a few times below solar. The $B-V$ and $V-K$ color gradients observed in the Cartwheel can be explained as a result of mixing of stellar populations born in a star-forming wave propagating through a low-metallicity gaseous disk, and a preexisting stellar disk of the size of the gaseous disk with color properties typical to those observed in nearby disk galaxies.

Subject headings: galaxies: individual (A0035−324) — galaxies: photometry — galaxies: stellar content — stars: formation

1. INTRODUCTION

Ring galaxies are believed to be the result of a head-on galaxy-galaxy collision. Such a collision generates an outwardly propagating wave of density enhancement in the disk of the larger galaxy, referred to as the target. Numerical models, starting from the pioneering paper of Lynds & Toomre (1976), confirm this picture. Simulations reproduce some of the basic features observed in ring galaxies, such as rings or crescent-shaped structures.

The density enhancements are likely to trigger star formation, and a ring of star formation is expected to form as a response to a circular density wave. The star-forming ring moves with time to progressively outer radii as the density wave propagates outward, and it leaves behind an evolved stellar population with the youngest stars located at the current position of the wave. The star formation history in a propagating wave is preserved, therefore, in the radial color distributions of stars in the disk. The inner disk is hence expected to be redder than its outer parts. Colors systematically reddening toward the center were indeed observed in the Cartwheel galaxy (Marcum, Appleton, & Higdon 1992, hereafter MAH), thus confirming this basic picture. More recently, similar radial color gradients were also found in other ring galaxies (Appleton & Marston 1997).

Although there seems to be good qualitative agreement between the collisional density wave model and the observed color gradients in ring galaxies, there is not yet a model of star formation that can quantitatively explain the observed color gradients. In their attempt to explain the color gradients in the Cartwheel, MAH had assumed a constant star formation scenario (Struck-Marcell & Tinsley 1978) and an instantaneous burst of star formation (Charlot & Bruzual 1991). The agreement between these models and the data is far from satisfactory. Both the models fail to reproduce the observed sequence of the reddening in the Cartwheel's disk. Part of this mismatch is likely due to a lack of consistency between the data and the models they used, as discussed below. MAH measured the color gradients in the Cartwheel in nine annuli with the width ≈ 1.3 kpc each. A wave propagating with the velocity of 60–90 km s^{-1} takes $(1.4–2.2) \times 10^7$ yr to cross an annulus. This is clearly inconsistent with the assumption of the instantaneous burst model that all the stars in an annulus were born simultaneously. The problem is more serious if the wave propagates more slowly. Constant star formation models assume an extended duration of star formation at each ring, whereas in an expanding density wave the star formation stops once the wave sweeps across that radius. Solar metallicity had been used in both models, whereas the Cartwheel's metallicity is about a tenth of solar (Fosbury & Hawarden 1977). The metallicity is one of the basic parameters that controls stellar evolution (Schaller et al. 1992), and hence color gradients are expected to depend on the metallicity.

In this paper we readdress the theoretical modeling of radial color gradients in ring galaxies, taking into account the age spread within a sampling annulus and the metallicity effects. We invoke two independent scenarios of star formation in ring galaxies. The first one is the conventional

[1] National Astronomical Observatory, Mitaka, Tokyo 181, Japan.

density wave scenario. In this scenario, the intruder's passage through the disk of the target galaxy creates a density wave that compresses the gas, thus inducing star formation. The star formation rate at each radius in this model is basically controlled by the strength of the density wave at that radius and the gas density. We use the Schmidt's law (Schmidt 1959) to relate star formation with the gas density. In the second scenario, we invoke a pure self-propagating star formation model, in which star formation is dissociated from the effects of the density wave model. An intruder has only a role of triggering the first event of star formation close to the point of impact; phenomena related to massive stars control the star formation at all other radii. As a particular case of the latter scenario we use the "fire in the forest" (FIF) model earlier applied for the interpretation of the surface brightness and the chemical abundance gradients in ring galaxies (Korchagin et al. 1998, 1999).

The kinematical data of ring galaxies seem to favor the density wave model for ring galaxies. However, the density wave model has a shortcoming in the case of the Cartwheel—none of the companion galaxies of the Cartwheel have enough mass to generate density waves strong enough to form a giant ring such as that observed in the Cartwheel (Davies & Morton 1982). New mass estimates have not improved the situation (Higdon 1996). Under the FIF scenario, star formation can be sustained subsequently even if the density wave is weak or totally absent. The FIF model completely neglects, however, any dynamical effects, which is a serious shortcoming of the theory. Both models, however, suit equally well our purpose to interpret optical color gradient in a radially propagating star-forming wave.

Although we treated the two scenarios as completely independent in this work, the two mechanisms may operate simultaneously. FIF phenomena can play a role even when a density wave by itself is strong enough to trigger star formation. The real situation may be a combination of the two scenarios.

In § 2, we formulate the models of star formation in ring galaxies. In § 3, we use these models to compute color-color diagrams for stellar populations born in the wave of star formation, propagating in a purely gaseous disk with different metallicities. In § 4, we discuss the comparison of the theoretical radial color gradients with the observed radial color gradients in the disk of the Cartwheel. The results are discussed in § 5.

2. STAR FORMATION SCENARIOS IN RING GALAXIES

2.1. *Density Wave–induced Star Formation*

Classical models of ring formation through collisions between galaxies predict an outwardly propagating circular density wave in the disk of the target galaxy. The density wave is expected to compress the gas, thus increasing the gas densities above the critical values required for star formation. We assume the star formation rate is proportional to the square of the density enhancement $\tilde{C}(r - Vt)$ propagating outwardly in a homogeneous gaseous disk. The balance of the surface density of stars (M_s) at a distance r from the center propagating with a velocity V and at time t can be then written as follows:

$$\frac{dM_s}{dt} = -D + kb\tilde{C}^2(r - Vt)\,, \tag{1}$$

with the density enhancement $\tilde{C}$ given by a Gaussian function:

$$\tilde{C}(r - Vt) = A \exp\left[-\frac{(r - Vt)^2}{l^2}\right]. \tag{2}$$

The first term D in the right-hand side of equation (1) gives the decrease of stellar density owing to the death of stars, and the second term describes the growth of density of stars as a result of star formation. The coefficients b and $k < 1$ determine the rate of star formation and its efficiency; l is the width of a star-forming ring.

Any dependence of the density enhancement on the strength of the density wave is not included in the above expression. Generally, the circularly expanding density waves are expected to change their amplitude with time. Numerical simulations by Athanassoula, Puerari, & Bosma (1997) and Struck-Marcell & Lotan (1990) show that the relative amplitude of the density wave remains near-constant during wave propagation. The amplitude of the density wave approximately follows the surface density profile of an unperturbed disk, which justifies our assumption of constant density wave amplitude for the flat surface density profile used in § 3. If the precollision Cartwheel was a normal disk galaxy with an exponential surface density distribution, the amplitude of the density wave should decrease more than an order of value when the wave reaches the present position of the outer ring of the Cartwheel.

2.2. *FIF Wave of Star Formation*

The propagation of FIF star formation wave in a gaseous medium with an initial surface mass density M_c is described by the following set of equations (Korchagin et al. 1998):

$$\frac{dM_s}{dt} = -D + kaM_c(\boldsymbol{x}, t - T)\int d\boldsymbol{x}' f(\boldsymbol{x} - \boldsymbol{x}')M_s(\boldsymbol{x}', t - T)\,, \tag{3}$$

$$\frac{dM_c}{dt} = -aM_c(\boldsymbol{x}, t)\int d\boldsymbol{x}' f(\boldsymbol{x} - \boldsymbol{x}')M_s(\boldsymbol{x}', t)\,. \tag{4}$$

Equations (3) and (4) give the rate of increase of surface density of the stars M_s and the corresponding decrease of surface density of the star-forming gas M_c, respectively. The first term D in the right-hand side of equation (3) describes the decrease of stellar density owing to the death of stars, and the second term describes the growth of density of stars as a result of induced star formation. The coefficients a and $k < 1$ determine the rate of star formation and its efficiency. The function f models the nonlocal "influence" of the star complexes located at point $\boldsymbol{x}'$ on the interstellar medium at point $\boldsymbol{x}$. This function has a characteristic "radius of influence" L, which, together with the characteristic time of the formation of stars T, controls the velocity of the star-forming wave.

2.3. *Model Parameters*

For the density wave scenario, computations were carried out for propagation velocities of 25, 55, 90, and 120

km s^{-1}. The efficiency of star formation k was taken to be 0.1. The amplitude A of the density wave was chosen to be $A = 1.5 \times 10^7\ M_\odot\ \mathrm{kpc}^{-2}$.

The set of parameters, as well as the particular choice of the function f for the FIF scenario, were taken from Korchagin et al. (1998). Specifically, $L = 2$ kpc, the delay parameter $T = 1.8 \times 10^7$ yr, and the efficiency of star formation $k = 0.1$. We refer the reader to Korchagin et al. (1998) for more details.

The parameters a and b determining the rate of star formation were chosen so as to reproduce the observed Hα surface brightness profile in the Cartwheel (Higdon 1995). This gives a value of $a = 0.75$ and $b = 0.025$ when masses, timescales, and distance scales are expressed in units of $10^7\ M_\odot$, 10^6 yr, and 1 kpc, respectively. With such values of parameters a and b, the theoretical rate of star formation in the wave is about $1.6 \times 10^{-7}\ M_\odot\ \mathrm{yr}^{-1}\ \mathrm{pc}^{-2}$, which is comparable to the estimated rate of star formation in the Cartwheel, $\sim 2 \times 10^{-7}\ M_\odot\ \mathrm{yr}^{-1}\ \mathrm{pc}^{-2}$ (Higdon 1995). Note that the colors of the star-forming waves are luminosity ratios by definition and do not depend on the free parameters controlling the rate of star formation.

The precollisional gas density is assumed to be uniform for purposes of studying the general color properties of the star-forming waves. In § 4.3, we discuss the effects of wave propagation in a medium with an exponentially decreasing density profile. The colors of the star-forming wave propagating in a medium with exponential surface density profile do not differ significantly from those computed for the flat surface density profiles.

3. COLOR GRADIENTS IN A STAR-FORMING WAVE

3.1. *Population Synthesis Model*

The mass M_s of stars formed per unit area is distributed into individual stellar masses using Salpeter's initial mass function (IMF) with $\alpha = 1.35$ and the stellar mass interval of $0.1\ M_\odot \le m_s \le 100\ M_\odot$. Once the IMF is fixed, the birth and death rates of stars can be determined at each radial grid zone from equations (1)–(4). The luminosity at a given band A after time t can be computed as

$$L_A(t) = \sum_m \sum_\tau l_A(m, \tau) N(m, \tau, t)\ , \qquad (5)$$

where $N(m, \tau, t)$ is the number of stars per unit surface area at time t with mass m and age τ, and $l_A(m, \tau)$ is the luminosity of a star in a band A. Stellar luminosities $l_A(m, \tau)$ are obtained using stellar evolutionary (Schaller et al. 1992) and atmospheric (Kurucz 1992) models. To determine the dependence of the color gradients on the chemical abundances in the star-forming gas, the initial metallicities adopted ranged from $Z_\odot/20$ to $2\ Z_\odot$. The population synthesis technique used in this work is explained in detail in Mayya (1995). The results of this code are compared with those from other existing codes by Charlot (1996). Recent updates in the code are described in Mayya (1997).

To study general color properties of stellar populations produced by the waves of star formation, we modeled the propagation of the density wave in a purely gaseous homogeneous disk. To do this, we divided the disk into 13 annuli with widths 1.25 kpc each. The first four annuli represent the "nucleus," and the outer annuli correspond approximately to the positions of annuli in Figure 1*a* of MAH. This approach was used for both the density wave and FIF wave models. Equations (1)–(5) were solved numerically, and the average colors were computed in each annulus, in the "nucleus" for the different velocities of the wave propagation, and for the different metallicities of the star-forming gas. Specifically, we computed color gradients produced by the wave, propagating with the velocities 25, 55, 90, and 120 km s^{-1}, and for the gas metallicities equal to $Z_\odot/20$, $Z_\odot/5$, $Z_\odot/2.5$, $Z_\odot$, and $2\ Z_\odot$.

3.2. *Results for Density Wave and FIF Wave*

Figures 1–4 show the results of these simulations for the density wave model at four different assumed velocities. Each frame in Figures 1–4 presents the color-color diagram computed for the moment when the star-forming wave reaches 16 kpc, the present position of the outer ring in the Cartwheel.

Two conclusions can be drawn from the theoretical color diagrams. Color properties of stellar populations produced by the wave of star formation do not depend strongly on the velocity of the wave but are sensitive to the heavy-element abundance of the star-forming gas. Stellar populations in

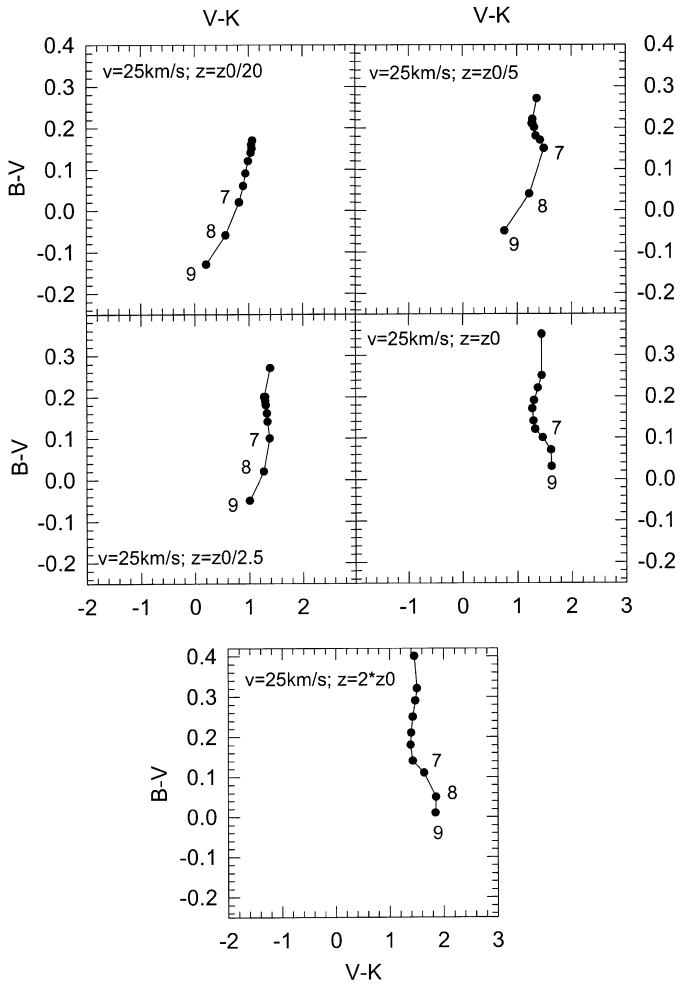

FIG. 1.—$B-V$, $V-K$ color plots computed for nine annular zones of a model ring galaxy. The star-forming density wave propagates with a velocity 25 km s^{-1} in a purely homogeneous gaseous disk. The plot illustrates the radial dependence of colors within the disk for five different metallicities of the star-forming gas: $Z_\odot/20$, $Z_\odot/5$, $Z_\odot/2.5$, $Z_\odot$, and $2\ Z_\odot$. Colors have regular reddening toward the disk center if the initial metallicity of gas is low.

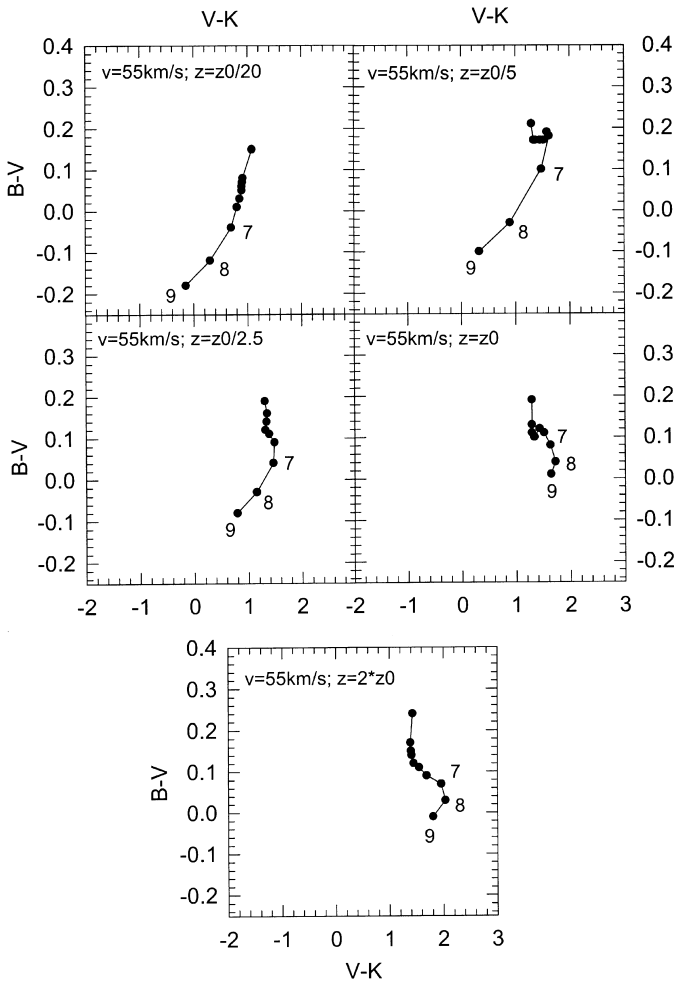

FIG. 2.—Same as in Fig. 1, but for a wave velocity of $v = 55$ km s^{-1}

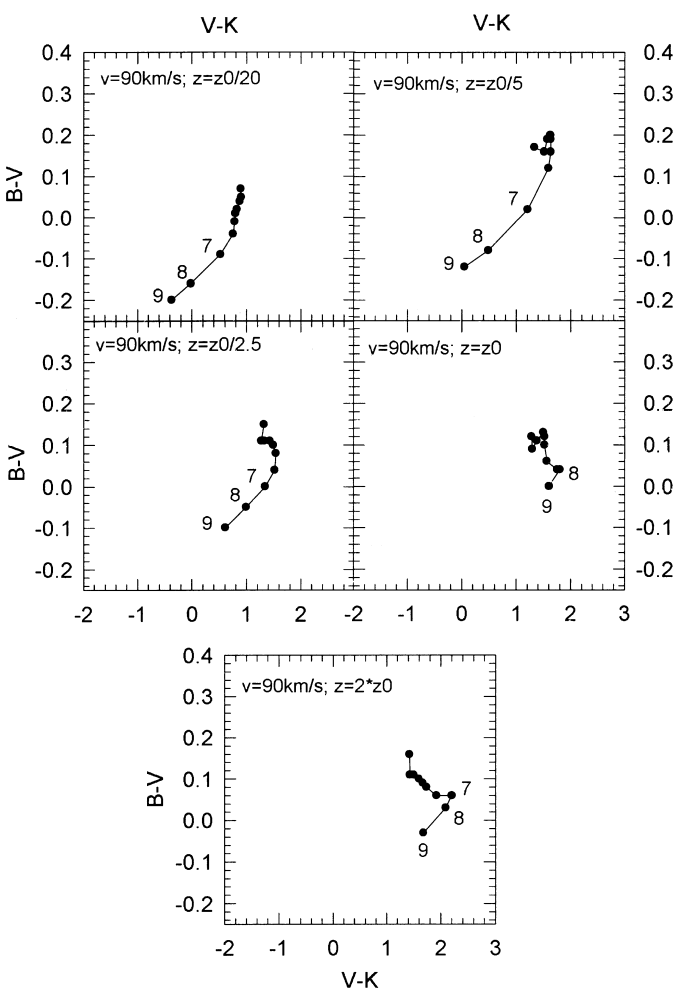

FIG. 3.—Same as in Fig. 1, but for a wave velocity of 90 km s^{-1}

the wake of the star-forming wave have spatially sequenced colors similar to those observed in the Cartwheel if the gas metallicity is subsolar. Figures 1–4 show that color diagrams do not have regular reddening toward the center of the disk if metallicity of the star-forming gas is solar or higher. This result is consistent with the measurements of the elemental abundances in the Cartwheel. In this galaxy, the heavy-element abundances are deficient by a factor of 10 as compared to the Orion Nebula (Fosbury & Hawarden 1977).

The origin of color sequentiality in a low-metallicity star-forming wave lies in the dependence of color-magnitude diagrams upon metallicity. Lowering Z causes individual stars to become both brighter and hotter. The relative contribution of supergiants to the total continuum considerably decreases with decreasing of metallicity. For example, the relative contribution of supergiants to the total continuum in R and V bands in a 5–20 Myr starburst is about 20%–80% for solar metallicity and decreases to 3%–40% for $Z = Z_{\odot}/10$ (Mas-Hesse & Kunth 1991). These factors, together with smoothing of colors by a noncoeval star formation in photometric rings, lead to the ordering of color-color diagrams in a low-metallicity gas. At solar metallicities photometric rings containing red supergiants break the spatial ordering of colors. Uncertainties of supergiant models do not allow us to make exact predictions, but the general trend of ordering of colors in a low-metallicity star-forming wave is robust.

For purposes of comparison, we also computed colors for an FIF scenario, in which all the effects of a density wave model are completely excluded. Figure 5 presents color diagrams for the FIF wave propagating with the velocity 90 km s^{-1} computed by solving equations (3)–(5). The IMF, stellar mass intervals, and the chemical abundances of the star-forming gas were chosen to be the same as in the density wave simulations shown in Figure 3. Comparison of these two figures further demonstrates that the color properties of stellar populations born in a star-forming wave do not depend on the particular mechanism of the wave propagation. This is because wave velocity and the present radius of the ring basically determine the mean age, and hence the color, of the stellar populations at a given radius.

We studied the dependence of color gradients on the particular choice of the initial mass function. Namely, we calculated color gradients for the Salpeter IMF with stellar mass interval of $0.5\ M_{\odot} \leq m_s \leq 50\ M_{\odot}$. Such an IMF produces more luminous stellar populations for a given stellar mass. Simulations show that colors are not much affected by the choice of the stellar mass intervals of IMF. However, the choice of IMF affects luminosities of stellar populations born in the wave. In general, radial color gradients are

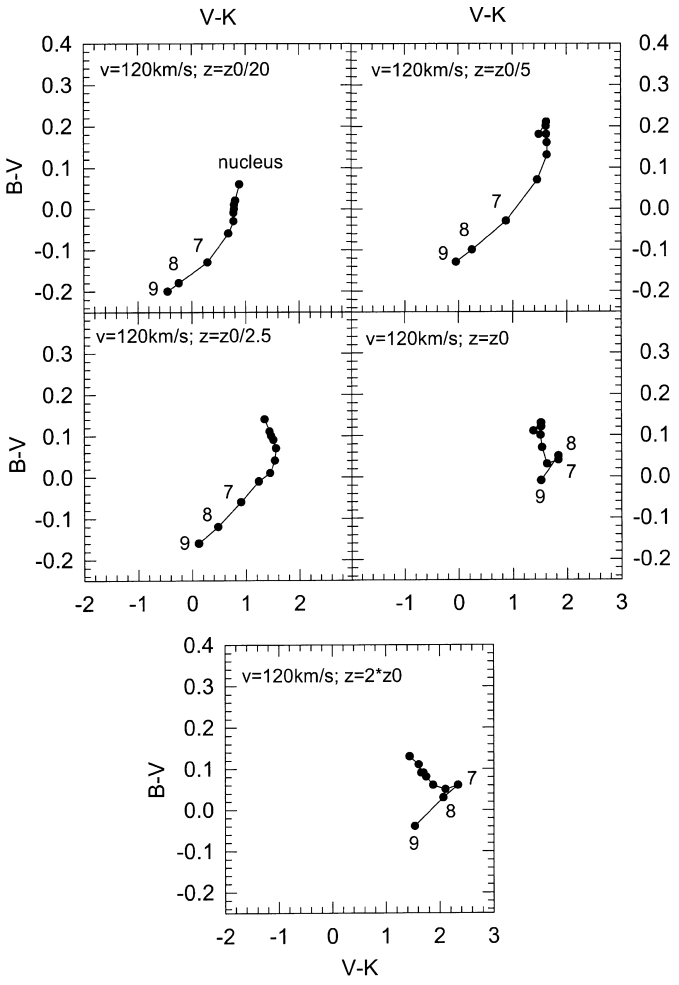

FIG. 4.—Same as in Fig. 1, but for a fast star-forming wave ($v = 120$ km s^{-1}).

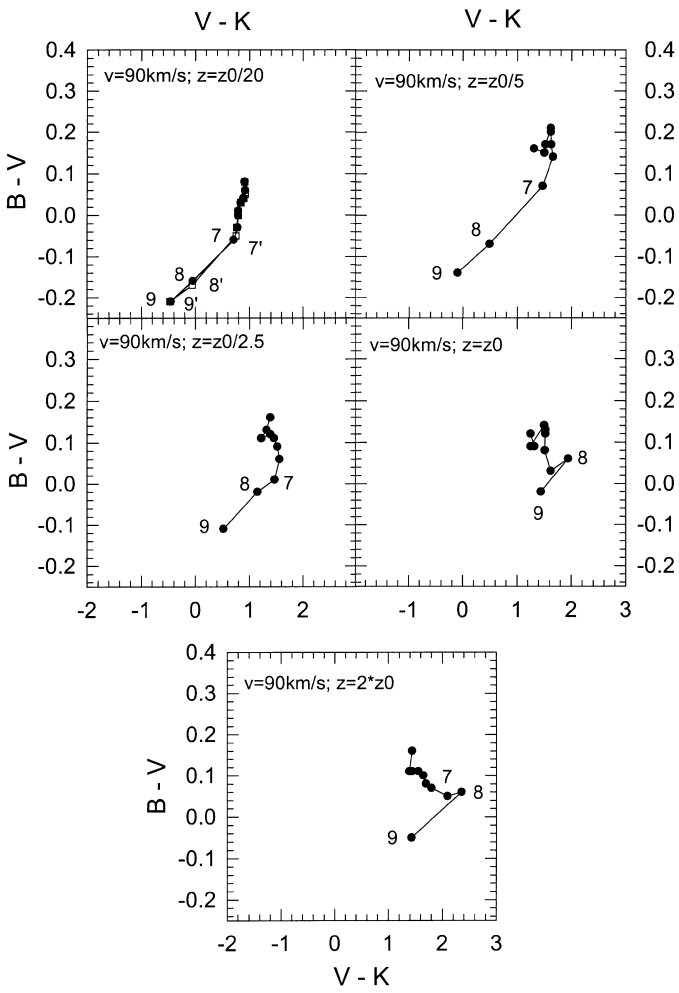

FIG. 5.—$B-V$, $V-K$ color plots computed for the FIF wave propagating with a velocity 90 km s^{-1}. The color diagrams for the FIF wave are similar to the color diagrams of the density wave propagating with the same velocity (Fig 3). The top left frame also shows a color diagram computed for the FIF wave propagating in the disk with an exponential surface density distribution (*open squares*) used for the modeling of the color properties of the Cartwheel galaxy.

strongly affected by abundance of heavy elements in the star-forming gas and to a less extent are affected by the radial velocity of the star-forming wave. Colors are insensitive to a particular mechanism of the star-forming wave and to the mass intervals of IMF.

4. APPLICATION TO THE CARTWHEEL

Theoretical colors in the wave are bluer compared to the colors observed in the Cartwheel galaxy (Fig. 8 of MAH), and hence the Cartwheel's colors cannot be explained by a wave of star formation propagating in a purely gaseous disk. This implies that a detailed modeling is required to fully understand the color gradients in the Cartwheel. In this section, we describe the method that we have adopted to explain the observed colors in the Cartwheel.

4.1. *Extinction Correction*

In principle, the redder colors of the Cartwheel compared to those of the expanding wave models can be the result of an increasing dust content toward the nucleus. There is evidence for both cold and warm dust in the Cartwheel. The cold dust is inferred from the *HST* images, which show a complicated network of dust lanes in the inner ring regions. The warm dust is inferred in the center regions and in part of the outer ring by ISOCAM observations (Charmandaris et al. 1999). However, there has not been an estimation of the extinction gradient from the above studies. The ISOCAM emission originates from nonequilibrium heating of very small grains and polycyclic aromatic hydrocarbons, which do not contribute much to the dust mass and hence to the optical extinction (Mayya & Rengarajan 1997). Therefore, even the high central emission in ISOCAM bands cannot be taken as evidence for a higher dust mass at the center.

We now investigate whether the observed gas densities in the Cartwheel are consistent with the assumption that the extinction plays a major role in creating an ordered color gradient. We hence estimated the color excess E_{B-V} on the basis of the hypothesis that the difference between the observed color gradient and that for the wave propagating on a purely gaseous disk can be completely explained by an extinction gradient. Details of the wave model that we used for the Cartwheel will be explained in § 4.3. Using the galactic dust/gas ratio (Bohlin, Savage, & Drake 1978), we then estimated the expected total surface density of gas $\Sigma^{\rm ext}_{\rm H\,I+H_2}$. The corresponding values of E_{B-V} for each annulus are listed in column (2) of Table 1, and the estimated surface densities of gas $\Sigma^{\rm ext}_{\rm H\,I+H_2}$ are given in column (3). Columns (4),

TABLE 1

GAS SURFACE DENSITIES ESTIMATED FROM THE MAXIMUM ALLOWED COLOR EXCESSES COMPARED WITH THE OBSERVED GAS SURFACE DENSITIES

Annulus (1)	$E(B-V)$ (mag) (2)	$\Sigma^{\rm ext}_{\rm H\,I+H_2}$ ($M_\odot$ pc^{-2}) (3)	$\Sigma^{\rm obs}_{\rm H\,I}$ ($M_\odot$ pc^{-2}) (4)	$\Sigma^{\rm obs}_{\rm H_2}$ ($M_\odot$ pc^{-2}) (5)	$\Sigma^{\rm obs}_{\rm H\,I+H_2}$ ($M_\odot$ pc^{-2}) (6)
Nucleus.....	0.62	27.1	$\leq$0.3	20–82	20–82
I.....	0.37	15.9	$\leq$0.3	20–82	20–82
II.....	0.34	14.8	4.5	...	4.5
III.....	0.27	11.8	4.5	...	4.5
IV.....	0.27	11.8	4.5	...	4.5
V.....	0.27	11.6	4.5	...	4.5
VI.....	0.26	11.4	4.5	...	4.5
VII.....	0.23	10.1	4.5	...	4.5
VIII.....	0.31	13.6	16.5	...	16.5
IX.....	0.36	15.7	16.5	...	16.5

(5), and (6) in Table 1 give the observed surface densities of atomic hydrogen $\Sigma^{\rm obs}_{\rm H\,I}$, molecular hydrogen $\Sigma^{\rm obs}_{\rm H_2}$, and the sum of atomic and molecular hydrogen $\Sigma^{\rm obs}_{\rm H\,I+H_2}$ in each annulus (Higdon 1996; Horellou et al. 1998). The annuli corresponding to the inner ring and two outer rings (VIII and IX) have the observed gas densities consistent with the extinction-estimated values. In the rest of the annuli, the extinction-estimated gas densities are overestimates, implying that the real extinction value is lower than that required to explain the observed colors. Hence, the extinction gradient cannot be responsible for the observed color gradient. An additional argument against large amounts of extinction is low metallicity of gas, which decreases the dust/gas ratio. This agrees with de Jong (1996), who found that the reddening because of dust does not play a significant role in the explanation of color gradients in the disks of spiral galaxies. The color gradients in galactic disks result from the combination of differences in stellar ages and the metallicity gradients across the disks.

The observed gas densities, on the other hand, can be used to derive the visual extinction at each annuli. The galactic dust/gas ratio gives us a value of 0.32 mag at annuli II–VII and 1.2 mag at the two outermost annuli. Using Balmer line ratios, Fosbury & Hawarden (1977) found the extinction in two outer H II regions to be $A_v = 2^{\rm m}.1$. Higdon (1996) derived an upper limit to visual extinction in two outer H II regions CW 17 and CW 23 of $A_v = 1^{\rm m}.6$ and $A_v = 2^{\rm m}.1$, which are consistent with the estimate by Fosbury & Hawarden (1977). Unfortunately, very little is known about the azimuthally averaged visual extinction, which is the directly relevant quantity for determining the corrections to the radial color gradients. The values reported by Fosbury & Hawarden (1977) and Higdon (1996) are greater than the observed visual extinction in other extragalactic H II regions. Kaufman et al. (1987) found an averaged value of $\langle A_v \rangle = 1^{\rm m}.1 \pm 0.4$ for 42 H II regions in M81. The azimuthally averaged visual extinction in the Cartwheel's outer ring can also be lower than the observed values for two most luminous H II regions. Visual extinction estimates based on the observed gas densities also give a lower value, which is closer to the value found by Kaufman et al (1987) than that estimated from Balmer lines. Note also that for $A_v = 2^{\rm m}.1$, the visual extinction correction to the observed colors in the two outer rings of the Cartwheel gives unrealistically blue colors. These colors are bluer than the theoretical colors of a very young (1 Myr) starburst. Therefore, we adopt in our calculations the values $A_v = 1^{\rm m}.2$ for the two outermost photometric rings, and $A_v = 0^{\rm m}.32$ for the rest of the photometric rings, following the estimates based on the observed gas densities.

4.2. *The Wave Velocity*

Even though the model colors are not strongly affected by the wave velocity, we discuss here the velocity adopted because of its importance for understanding the physical nature of the star-forming waves.

There have been studies of kinematical motions in the Cartwheel galaxy using different techniques. Fosbury & Hawarden (1977) used optical long-slit spectroscopic data, Higdon (1996) used H I data, and more recently Amram et al. (1998) used Hα Fabry-Perot data. A standard method of interpretation of motions in the ring galaxies assumes that all the internal motions are in the plane of the ring and that the kinematical motions can be represented by a systematic motion of the galaxy together with ring's rotation and its expansion. Using this method, different authors obtain rather different values for the expansion velocity of matter in the outer ring of the Cartwheel galaxy. Fosbury & Hawarden (1977) used optical spectroscopy of five H II regions and found a radial expansion velocity of 89 ± 40 km s^{-1}. Higdon (1996) finds that the outer ring is expanding with the velocity 53 ± 9 km s^{-1}. Amram et al. (1998) using the best spatial resolution and a much larger number of points compared to the previous studies find the velocity of expansion (13–17) $\pm$ 2 km s^{-1}. With a slightly different approach, Amram et al. find the value of the matter expansion to be 30 ± 10 km s^{-1}. This value is in poor agreement with the value 53 ± 9 km s^{-1} found by Higdon (1996). The authors notice, however, that cold and ionized gas might suffer different expanding phases.

It must be stressed that all these measurements determine the internal motions of cold or ionized gas in the wave of star formation and do not determine the velocity of propagation of the wave itself. This is exactly similar to the kinematical studies of spiral density waves, where the measured motions within the spiral arms themselves (i.e., the streaming motions) determine the amplitude of spiral density waves and do not give the pattern speed of the wave. In our modeling, we therefore based the choice of the propagation velocity of the star-forming wave on the best fit for the surface brightness distributions in the disk of the Cartwheel. Korchagin et al. (1998) found that the observed Hα and red

continuum surface brightness distributions are well reproduced for the velocity of the wave of about 90 km s^{-1}.

4.3. *Color Gradients in the Cartwheel*

The color gradients that were presented in the previous section assumed a homogeneous gaseous disk. The majority of galaxies have exponentially decreasing gas surface density profiles. Nevertheless, the above calculations adequately illustrate the basic dependence of color gradients as a function of the wave velocity and metallicity. To calculate the color gradients in the Cartwheel, we used an exponential gas surface density profile

$$\sigma_c(r) = A \exp\left(\frac{-r}{H}\right) \quad (6)$$

with the parameters $A = 1.5 \times 10^8\ M_\odot$ kpc^{-2} and $H = 6.5$ kpc, which are typical for the late-type spirals (Tacconi & Young 1986). The initial metallicity of gas was chosen to be 1/20 of the solar metallicity, close to the values observed for the outer ring by Fosbury & Hawarden (1977).

An FIF wave propagating in an inhomogeneous medium has a nonconstant velocity that affects the ages of stellar populations behind the star-forming wave and, hence, their color properties. The change in the wave velocity owing to the radial variation of surface density is within 12% of the mean value 94 km s^{-1} throughout the disk of the Cartwheel. The resulting model color-color diagram is shown in Figure 6. Colors do not differ significantly from those computed in the previous section (see the top left plot in Fig. 5). Figure 6 also includes the extinction-corrected colors observed in the Cartwheel (*filled triangles*). The extinction corrections were based on the gas column density and the galactic $A_v/N_{\rm H}$ ratio as explained in the previous subsection. Specifically, the observed colors for the two outer photometric rings were corrected for the extinction $A_v = 1^{\rm m}.2$, and the rest were corrected for the extinction value $A_v = 0^{\rm m}.32$. The model reproduces the sequence of points in the color-color diagram. However, $V-K$ colors in the wave are around 1 mag bluer than the observed colors of the Cartwheel galaxy. Hence, the color properties of the stellar populations born in a purely star-forming wave together with the extinction correction cannot entirely explain the observed colors. This is not unexpected, because the precollisional stellar disk is known to have a nonnegligible contribution to the colors of the Cartwheel.

Optical color gradients are common among "normal" disk galaxies. Figure 7 shows $B-V$ versus $V-K$ color profiles in the disks of six nearby galaxies that were plotted using de Jong's (1996) observational data. The observed colors of spiral galaxies are even redder than the observed colors in the Cartwheel. This indicates that the Cartwheel's colors can indeed be obtained by mixing stellar populations born in the wave with the older stellar populations existing in the Cartwheel's disk before the collision.

Color mixing cannot be considered separate from the surface brightness constraints. The spatial distribution of the young stellar population can be found from the best fit

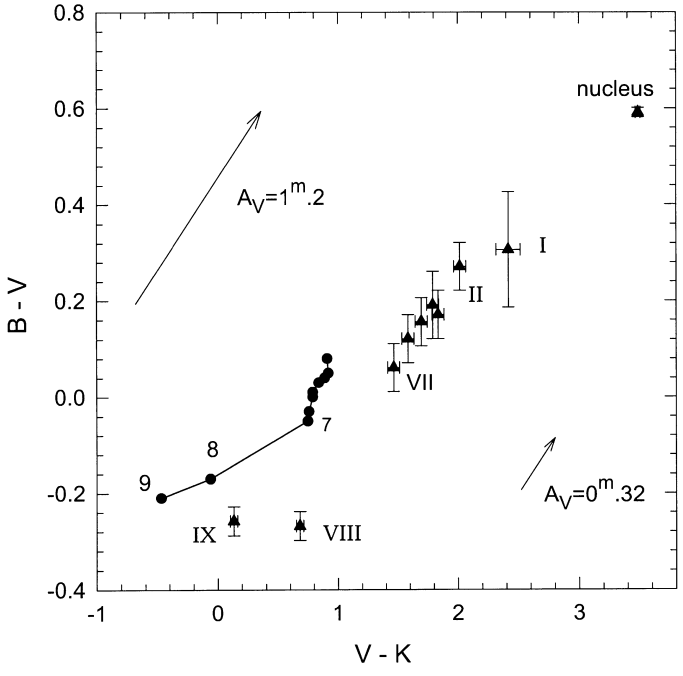

FIG. 6.—Model ring galaxy colors compared with the observed colors of the Cartwheel. The large filled triangles mark the $B-V$, $V-K$ colors observed in the Cartwheel galaxy (MAH). The colors of the two outer photometric rings, VIII and IX, were corrected for extinction using $A_v = 1^{\rm m}.2$. The colors of the inner photometric rings and the Cartwheel's nucleus were corrected using $A_V = 0^{\rm m}.32$. The filled circles show the $B-V$, $V-K$ colors produced by the star-forming wave propagating in a purely gaseous ($Z_\odot/20$) disk with the velocity 90 km s^{-1}. The model colors are bluer than the observed colors in the Cartwheel. The values of extinction correction are shown by the arrows.

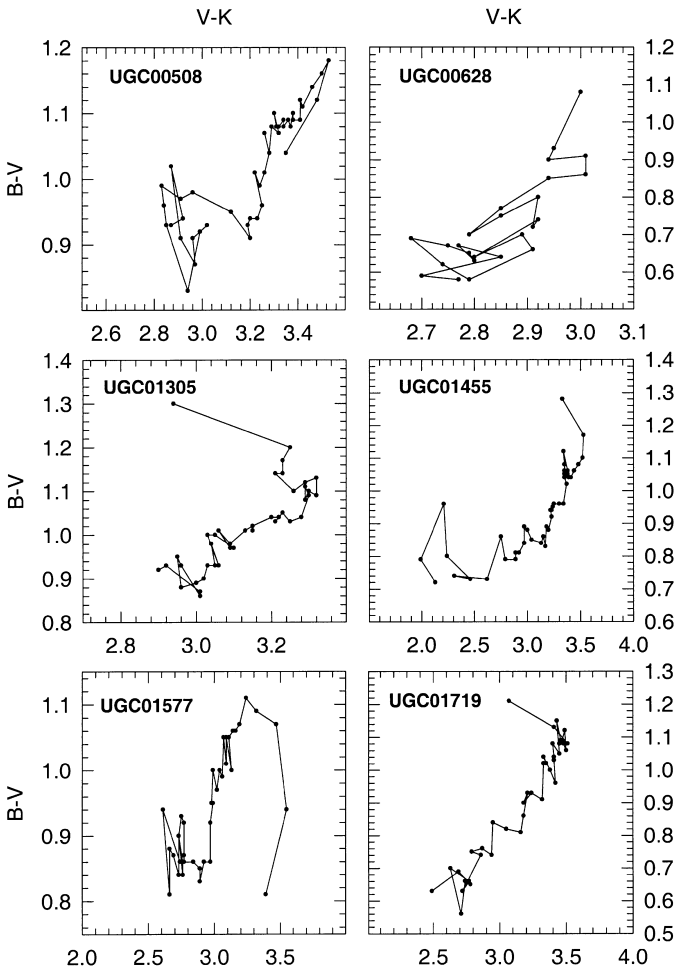

FIG. 7.—Color-color ($B-V$, $V-K$) plots of six disk galaxies as measured by de Jong (1996).

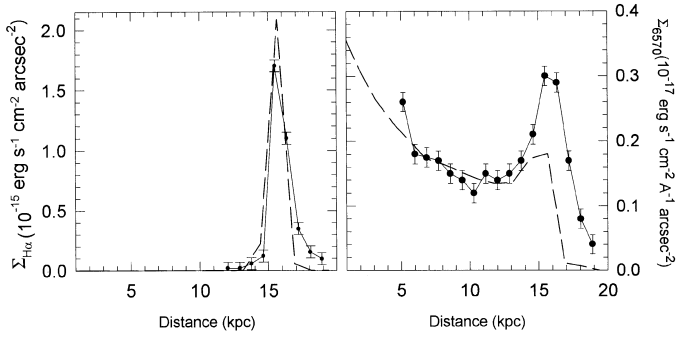

FIG. 8.—Red continuum and Hα surface brightness distributions produced by the wave of star formation propagating in a gaseous disk with exponential surface density profile with the parameters $A = 5 \times 10^7\ M_\odot$ kpc^{-2}, $H = 11$ kpc, and gas metallicity $Z_\odot/20$. An underlying old stellar disk with $\mu_0(V) = 23.5$ mag arcsec^{-2} and $R_0 = 5$ kpc is added to the model ring galaxy.

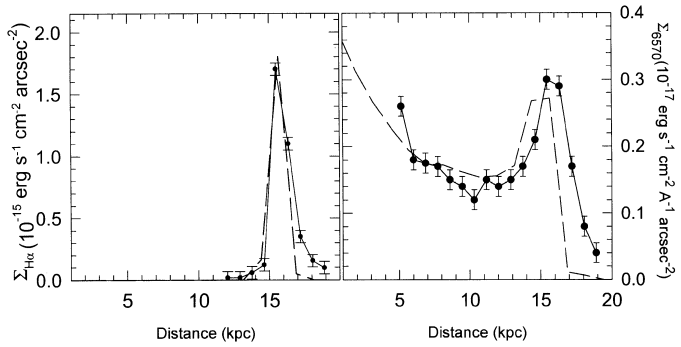

FIG. 9.—Red continuum and Hα surface brightnesses in the wave with the same parameters employed in Fig. 8, but with metallicity $Z_\odot/5$.

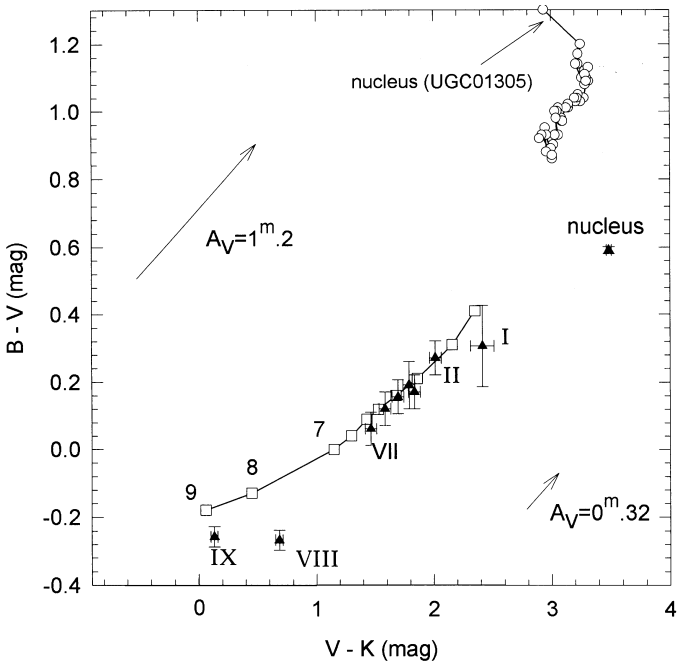

FIG. 10.—Model colors computed for the wave of star formation propagating in a gaseous disk with the parameters employed in Fig. 8. An underlying disk is added to the model ring galaxy. The large filled triangles mark the extinction-corrected colors of the Cartwheel galaxy. The open circles indicate the observed colors for galaxy UGC 01305. The open squares show the colors obtained as a result of mixing of the colors produced by the star-forming wave propagating in a purely gaseous ($Z_\odot/20$) exponential disk, with the observed colors in UGC 01305. The mixed colors are close to the observed ones in the Cartwheel.

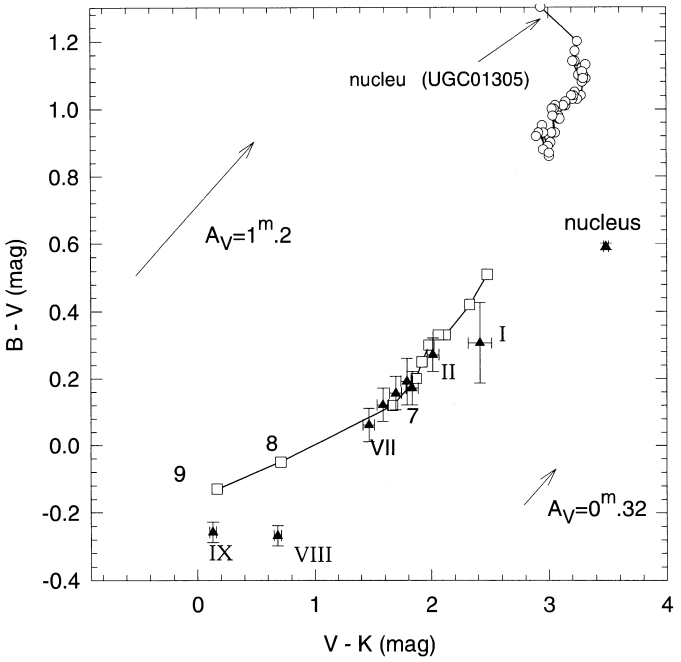

FIG. 11.—Same as in Fig. 10, but for the initial metallicity of the gaseous disk $Z_\odot/5$

to Hα surface brightness distribution in the Cartwheel. Assuming exponential gas surface density distribution we find that the best fit to Hα surface brightness distribution in the Cartwheel (Fig. 8) can be obtained for the FIF wave propagating in the gaseous disk with the parameters $A = 5 \times 10^7\ M_\odot$ kpc^{-2}, and $H = 11$ kpc. For the old stellar population in the Cartwheel, we assumed that it has an exponential distribution in the V band. Specifically, we

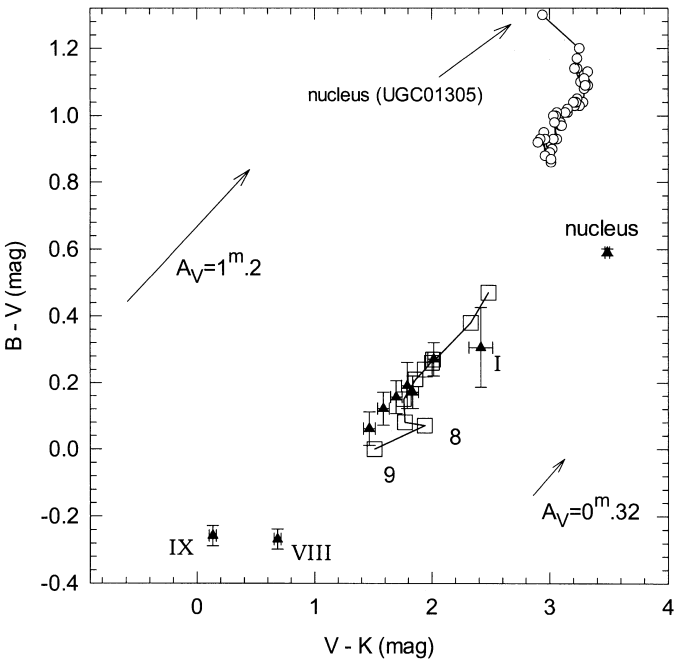

FIG. 12.—Model colors computed for the model with the parameters employed in Figs. 10 and 11, but for the initial metallicity of the gaseous disk $Z = Z_\odot$. The observed colors are in disagreement with the Cartwheel's observations, suggesting a low metallicity for the star-forming gas in the Cartwheel.

assumed that V-band surface brightness $\mu(r)$ at a distance r from the galactic center is given by the relation $\mu(r) = \mu_0 + 1.086r/R_0$, where μ_0 is the surface brightness in the center of the disk in mag arcsec^{-2}, and R_0 determines the scale length of the exponential surface brightness distribution. Choosing $R_0 = 5$ kpc, which is the typical value for disk galaxies (de Jong 1996), we find that the best fit to the red continuum profile in the Cartwheel can be obtained for $\mu_0 = 23.5$ mag arcsec^{-2}. The red continuum brightness distribution, however, is in a poor agreement with observations. The maximum of the red continuum peak associated with the outer ring of the Cartwheel is less prominent as compared to observations. Higher gas metallicities increase a relative contribution of supergiants to the total continuum. Figure 9 shows Hα and red continuum surface brightness profiles for the same parameters as in Figure 8 but for the metallicity of gas $Z_\odot/5$, which gives more satisfactory fit to observational data.

The surface brightness profiles were then used to calculate the luminosity of precollisional stellar disk of each radial zone. The total luminosity of each zone is obtained by summing the luminosities of pre- and post-collisional stars, which were then used to calculate the color profiles. The precollisional stellar disk seems to lack any bulge, and hence the Cartwheel was most probably a late-type spiral (Higdon 1996). We assume that the preexisting old disk of the Cartwheel has color properties typical to those in the late-type disk galaxies. As an example we used de Jong's (1996) color profiles for the Sbc galaxy UGC 01305. The resulting color profiles are plotted in Figures 10 and 11 for $Z_\odot/20$ and $Z_\odot/5$ metallicities, respectively. The filled triangles in the figures indicate the extinction-corrected observed colors of the nine rings in the Cartwheel's disk and its nucleus. The colors of galaxy UGC 01305 are marked by open circles. The resulting colors of the mixed stellar populations are shown by the open squares. The outer three radial zones 9, 8, and 7 are identified for both the observed and model points. It can be seen that the observed colors are best reproduced in the model with exponentially decreasing gas surface density distribution and with metallicity of gas $Z_\odot/20$ (Fig. 10). This model, however, does not reproduce well the red continuum surface brightness profile. The model with the metallicity of the star-forming gas $Z_\odot/5$ satisfactorily reproduces the range of the observed colors and their spatial sequence. This is not the case if the metallicity of the stars formed in the wave was solar, as illustrated in Figure 12. All the notations of the previous figure are retained, and hence the open squares represent the mixed model colors. This model explains neither the range of observed colors nor the spatial sequence of the colors.

5. SUMMARY AND DISCUSSION

This paper has focused on the optical properties of disk galaxies with large-scale star-forming rings. We considered an improved model of a star-forming wave and used the population synthesis approach to calculate the disk color gradients produced by an outwardly propagating wave of star formation. The results of our calculations can be summarized as follows:

1. Subsolar metallicities (by at least a factor of 2.5) are necessary for generating color profiles that redden systematically toward the center. This result is consistent with the observed metallicity in the Cartwheel, where such color gradients are observed.

2. The theoretical colors of the stellar populations born in the wave propagating in a purely gaseous disk are much bluer than the observed colors of the Cartwheel's disk. A reddening gradient caused by interstellar dust cannot explain the discrepancy. Instead, an explanation of the Cartwheel's colors requires the presence of an old stellar disk extending out to the present position of the ring. The existence of a precollisional nucleus in the Cartwheel has been known for more than two decades, but this is the first unambiguous evidence for a large stellar disk in the Cartwheel.

Simple models used in this paper leave aside many important aspects of the dynamics of ring galaxies. They allow us, however, to make a conclusion on the nature of a precollisional Cartwheel galaxy. Higdon (1996) assumed that a precollisional Cartwheel would have appeared as a small spiral embedded in an extensive low surface density H I disk. Our results show that the old stellar populations must exist in the entire disk of the Cartwheel in order to understand the observed color gradients.

These conclusions raise the question of the survival of the precollisional disk structure during an encounter. Athanassoula, Puerari, & Bosma (1997) numerically studied collisions of intruders with barred disk galaxies. They found that an intruder with mass equal to 10% of the mass of a target barred galaxy leaves the bar undestroyed. To our knowledge, there is no study of the collisional disruption of disk galaxies that have well-developed spiral structure. The stability properties of gravitating disks can be drastically changed by a few percent admixture of cold gas. If the precollisional disk of the Cartwheel was gas rich, and most of the gas was burnt in the star-forming wave or stripped from the galactic plane, any precollisional spiral structure would not have survived. All these questions remain for future investigations.

The authors thank the anonymous referee for his or her useful comments, W. Wall for reading the manuscript, which resulted in improved presentation, and Roelof de Jong for providing his observational data in electronic form. V. K. acknowledges S. Miyama for his hospitality and the National Astronomical Observatory of Tokyo for providing a COE fellowship. This work has been partly supported by CONACyT research grant 211290-5-25869E.

REFERENCES

Amram, P., Mendes de Oliveira, C., Boulesteix, J., & Balkowski, C. 1998, A&A, 330, 881
Appleton, P. N., & Marston, A. P. 1997, AJ, 113, 201
Athanassoula, E., Puerari, I., & Bosma, A. 1997, MNRAS, 286, 284
Bohlin, R. C., Savage, B. D., & Drake, J. F. 1978, ApJ, 224, 132
Charlot, S. 1996, in ASP Conf. Ser. 98, From Stars to Galaxies, ed. C. Leitherer, U. Fritze-von Alvensleben, & J. Huchra (San Francisco: ASP), 275
Charlot, S., & Bruzual, A. 1991, ApJ, 367, 126
Charmandaris, V., Laurent, O., Mirabel, I. F., Gallais, P., Sauvage, M., Vigroux, L., Cesarsky, C., & Appleton, P. N. 1999, A&A, 341, 69
Davies, R. L., & Morton, D. C. 1982, MNRAS, 201, 69P
de Jong, R. S. 1996, A&A, 313, 377
Fosbury, R. A. E., & Hawarden, T. G. 1977, MNRAS, 178, 473
Higdon, J. L. 1995, ApJ, 455, 524
———. 1996, ApJ, 467, 241
Horellou, C., Charmandaris, V., Combes, F., Appleton, P. N., Casoli, F., & Mirabel, I. F. 1998, A&A, 340, L51

Kaufman, M., Bash, F. N., Kennicutt, R. C., Jr., & Hodge, P. W. 1987, ApJ, 319, 61
Korchagin, V., Mayya, Y. D., Vorobyov, E. I., & Kembhavi, A. K. 1998, ApJ, 495, 757
Korchagin, V., Vorobyov, E. I., & Mayya, Y. D. 1999, ApJ, 522, 767
Kurucz, R. L. 1992, in IAU Symp. 149, Stellar Populations of Galaxies, ed. B. Barbuy & A. Renzini (New York: Kluwer), 225
Lynds, R., & Toomre, A. 1976, ApJ, 209, 382
Marcum, P. M., Appleton, P. N., & Higdon, J. L. 1992, ApJ, 399, 57
Mas-Hesse, J. M., & Kunth, D. 1991, A&AS, 88, 399
Mayya, Y. D. 1995, AJ, 109, 2503
———. 1997, ApJ, 482, L149
Mayya, Y. D., & Rengarajan, T. N. 1997, AJ, 114, 946
Schaller, G., Schaerer, D., Meynet, G., & Maeder, A. 1992, A&AS, 96, 269
Schmidt, M. 1959, ApJ, 129, 243
Struck-Marcell, C., & Lotan, P. 1990, ApJ, 358, 99
Struck-Marcell, C., & Tinsley, B. M. 1978, ApJ, 221, 562
Tacconi, L. J., & Young, J. S. 1986, ApJ, 308, 600